Use of nano-magnetic materials for removal of Congo red dye from aqueous solutions

Article *in* Advances in Natural Sciences Nanoscience and Nanotechnology · April 2025

DOI: 10.1088/2043-6262/adc977

5 authors, including:

Ahmed Yousif Hammood
University of Basrah
14 PUBLICATIONS **24** CITATIONS
SEE PROFILE

Muhand K. Al-Tememi
University of Basrah
13 PUBLICATIONS **63** CITATIONS
SEE PROFILE

Ahmed A. Majed
University of Basrah
16 PUBLICATIONS **39** CITATIONS
SEE PROFILE

IOP Publishing Advances in Natural Sciences: Nanoscience and Nanotechnology
Adv. Nat. Sci.: Nanosci. Nanotechnol. **16** (2025) 025014 (8pp) https://doi.org/10.1088/2043-6262/adc977

Use of nano-magnetic materials for removal of Congo red dye from aqueous solutions

Ahmed Yousif Hammood[1], Muayad H M Albehadili[2], Muhand K AL-Tememi[1], Ahmed A Majed[3,4] and Wejdan Ali Radhi[5]

[1] Marine Science Center, University of Basrah, Basrah, Iraq
[2] College of Marine Science, University of Basrah, Basrah, Iraq
[3] College of Education for Pure Science, University of Basrah, Iraq
[4] Scientific Research Center, Al-Ayen University, Thi-Qar, Iraq
[5] Basra Education Directorate, Ministry of Education, Basrah, Iraq

E-mail: eduppg.ahmed.majed@uobasrah.edu.iq

Received 3 December 2024
Accepted for publication 2 April 2025
Published 24 April 2025

Abstract

Sol–gel auto-combustion was used to create ferrite nanoparticles with the structure $Co_{0.5}Cr_{0.5}Fe_2O_4$ using lemon juice as a fuel agent and surfactant. It was investigated whether the generated nanomaterials could absorb Congo red dye. Different techniques were used to characterize the prepared nanocomposite x-ray diffraction (XRD), FE-SEM, EDX, FT-IR and Zeta Potential. The XRD characterization proved the phase purity of the prepared material, the particle size was 28.34 nm. The study dealt with the use of the prepared compound as an adsorbent surface for Congo red dye from its aqueous solutions. Freundlich and Langmuir equations were applied to the adsorption process data for different temperatures. The results showed that the Langmuir equation is more linear than the Freundlich equation. In addition, the thermodynamic results showed that the adsorption of Congo red dye was spontaneous, as the value of (ΔG) was negative at low concentrations before turning to a positive value with increasing concentrations. Also, the adsorption process was endothermic and increased in randomness through the positive value of (ΔS). The adsorption results showed that equilibrium was reached in 300 min and that the removal of Congo red dye constituted 84.24% of the total. The possibility of reusing the prepared compound several times was studied, and the results showed the possibility of activating the surface while maintaining its properties as a good adsorbent surface.

Keywords: adsorption, Congo red dye, ferrite nanoparticles, Langmuir and Frendlich, thermodynamic
Classification numbers: 2.03, 5.02

1. Introduction

The aquatic environment suffers from various types of pollutants, such as heavy metals, dyes, petroleum products, and the products of various industrial activities that are mainly untreated and make their way into the aquatic environment. Thousands of chemicals may be used in industrial processes that include a large number of organic and inorganic compounds that are released into the environment. Watercolor [1], Exposure of the aquatic environment to this huge amount of pollutants of various types and forms leads to pollution and destruction of life forms in it as a result of the transformation of these pollutants into more complex forms, causing short or long-term toxic effects that may in turn lead to a negative impact on living organisms, including humans, and makes water Not suitable for required uses [2, 3].

Organic dyes are one of the most important water pollutants and are currently estimated at more than one hundred thousand commercially available dyes, amounting to more than (7×10^5) tons of dyes produced annually [4]. The amount of dyes that are consumed in the textile industry and around the world is estimated at more than (10 000 tons) annually, and about (1%) of these dyes are discharged into water channels annually, and accurate data on the amount of

dyes that are discharged from various industries into the environment is not known. It is well known, however, that the release of industrial dyes into the environment has presented challenges to environmental scientists [5]. Many dyes are toxic and carcinogenic and therefore affect the life of living organisms and cause a direct impact on the life of these organisms [6]. These dyes also contribute to water pollution and represent an increasing danger to the environment, aquatic life, and to humans and animals [7]. When dyes resulting from industries are secreted into the water of rivers and lakes, even if they are in small quantities, they will affect the physical and chemical properties of the water and lead to a decrease in the concentration of dissolved oxygen, which then leads to cases of oxygen deficiency and as a result affects the life of aquatic organisms [8]. Congo red is one of the diazo dyes that is water-soluble and stable [9]. It is considered one of the dangerous dyes for different living things, as this dye is derived from benzidine and naphthoic acid. Human exposure to high concentrations of this dye leads to cancer. It may cause allergies to the eyes and skin, irritate the nervous system, affect blood factors such as clotting, and have other effects on human health that are unknown [10]. Congo red dye has wide uses in many industries such as textiles, papers, rubber, plastics and other industries. It is the first industrial dye that has the ability to dye cotton directly. This dye is Affected to changes in pH value, as its color changes in acidic and basic environments [11]. Congo red is one of the industrial dyes that is tricky to break For its stability chemical-physical and thermal. It is also characterized by its high solubility in water, which makes the process of treating or removing this dye from water contaminated with it very difficult [12]. For this reason, it is crucial to use economical, efficient, and ecologically friendly treatment techniques to clean up dye-containing waters and wastewater. Adsorption is the most widely used method for depolluting dye-contaminated waters out of all the approaches, The methods include physical (adsorption, filtration, ion exchange, etc) and chemical methods (agglomeration, coagulation, oxidation, etc). Adsorption is made possible by its wide range of available natural and artificial adsorbent materials and its simplicity [13, 14]. Recently, the development of innovative and low-cost nanomaterials has received wide attention for various applications, including the treatment and detection of pollutants, as well as water purification using nanoparticles as nanofilters, as well as various uses resulting from the advancement of this technology [15, 16]. Recently, spinel ferrites have been developed as new and effective adsorbents for water pollution treatment [17, 18]. Because of its active sites and large surface area, it is an effective material in removing impurities. Due to their exceptional superparamagnetic qualities, spinel ferrites are easily extracted from reaction mixtures using an external magnetic field (SPM) [19, 20]. The ability to remove organic pollutants, hazardous metals and nutrients from polluted water has been verified [21]. Spinel ferrites have the general formula MFe_2O_4, where M represents one of the divalent elements that belong to the transition elements in the periodic table such as (Fe^{2+}, Cu^{2+}, Zn^{2+} Co^{2+}, Ni^{2+}, Cd^{2+}, etc) or a mixture of them. The unit cell of spinel ferrites contains 32 oxygen ions, and these ions represent the basic reaction unit, as positive ions are linked to them, thus forming the cubic lattice. There are 96 sites among the oxygen ions, of which 64 are tetrahedral (A) and 32 are octahedral (B). The ability to remove magnetic spinel ferrites is strengthened by their high surface area and smaller particle size when they are made into nanoparticles [22]. There are many methods used to prepare magnetic nano spin ferrites, such as precipitation method [23, 24], the hydrothermal method [25], the sol–gel method [26] and the sol–gel auto- combustion method [27]. In the present study, natural lemon juice was used as a reaction fuel and as a surface active agent to produce cobalt ferrite and zinc ferrite using the spontaneous combustion sol–gel method, which is an environmentally friendly and less expensive technique and is considered one of the green chemistry methods. The current study aims to provide a nano-adsorbent surface to remove Congo red dye from its aqueous solutions. The study proved the possibility of using the prepared compound to remove the dye and the possibility of reusing it again.

2. Materials and methods

2.1. Synthesis of $Co_{0.5}Cr_{0.5}Fe_2O_4$ nanoparticles

The compound $Co_{0.5}Cr_{0.5}Fe_2O_4$ was prepared as follows:

- 14.54 g of $Fe(NO_3)_3{\cdot}9H_2O$ (99.8%; Merck) with 2.63 g of $Co(NO_3)_2{\cdot}6H_2O$ (96%; Aldrich)with 3.60 g of $Cr(NO_3)_2{\cdot}9H_2O$ (96%; Aldrich) were weighed and placed in a beaker and (45 ml) of lemon juice was added and then the materials were mixed using a magnetic stirrer.
- Ammonium hydroxide was added to the solution during the mixing process to adjust the pH to (7), then the solution was mixed for (30 min) for the purpose of homogeneity.
- Then the temperature was raised to 150 °C until the solution was completely converted into a gel. After a short period of time, the gel began to burn until it became a dry powder. After that, the dry gel was ground.
- The ferrite powder was calcined at 600 °C for (3 h) in order to remove the remaining materials in the ferrite such as organic compounds, carbon oxides and water.

2.2. Characterization techniques

The prepared compound was characterized using several techniques, including (FESEM) scanning electron microscopy, x-ray diffraction (XRD), Fourier transform infrared spectroscopy, energy dispersive x-ray detection (EDX), and ultraviolet–visible spectroscopy was used to calculate the dye concentrations.

2.3. Adsorption studies

In order to find the exact concentrations of Congo red dye, a standard solution was prepared with a concentration of (1000 mg l^{-1}) and then used to prepare standard solutions within the range (2–30 mg l^{-1}). The time required to reach equilibrium was studied by taking different time periods within the range (15–360 min) at a temperature of (25 °C), where an initial concentration and initial volume of the dye were used (20 mg l^{-1}, 25 ml) and a constant weight of the material for the nanocomposite (0.05 g) at a shaking speed of (120 rpm). The acid function was studied within the range (5–9) using sodium hydroxide (0.1 M) and hydrochloric acid with a concentration of (0.1 M). Equations (1) and (2) were used to calculate the adsorption capacity (Q_e) and the percentage of adsorption ($R\%$) [28].

$$Q_e = V(C_0 - C_e)/m \tag{1}$$

$$\text{removal } \% = [(C_0 - C_e)/C_0] \times 100, \tag{2}$$

where: m is the weight of the adsorbent (g), Q_e is the adsorption capacity of the adsorbent surface (mg g^{-1}), V is the volume of the adsorbent (l), C_0 is the initial dye concentration in mg l^{-1}, C_e = the residual dye concentration in mg l^{-1}.

2.4. Thermodynamic parameters

The values of the functions ΔG, ΔH, and ΔS were calculated using equations (3)–(5) by taking concentrations in the range of (10–50 mg l^{-1}) of Congo red dye. The concentrations were added to flasks containing a weight of (0.05 g) of $Co_{0.5}Cr_{0.5}Fe_2O_4$, then shaken at a speed of (120 rpm) for the required period of time at different in the range of (10.0, 25.0, 37.5, and 50.0 °C). Then the solutions were separated and the remaining concentrations of the dye were calculated.

$$\Delta G = -RT \ln K \tag{3}$$

$$K = C_{\text{solid}}/C_{\text{liquid}} \tag{4}$$

$$\ln K = \Delta S/R - \Delta H/RT, \tag{5}$$

where C_{solid} is the concentration in the solid phase at equilibrium in units of (mg l^{-1}), C_{liquid} is the concentration in the liquid phase at equilibrium in units of (mg l^{-1}), ΔG represents the Gibbs free energy (KJ mol^{-1}), T is the temperature in Kelvin, R is the gas constant (0.0083 KJ K^{-1} mol^{-1}) [29].

2.5. Method of reactivating the surface of the absorbent

For the purpose of reactivating and using the absorbent surface and recovering the dye from the surface, the volume and concentration of Congo red dye (50 ml, 150 mg l^{-1}) were taken and added to a weight of (0.05 g) of the absorbent surface. Then the solution was placed in a shaking incubator at a speed of (120 rpm) and a temperature of (25 °C) and an equilibrium time of (300 min), after which the adsorbent material was separated using a magnet, then (25 ml) of ethyl alcohol was added to the adsorbent surface and the shaking process was carried out for equilibrium time of 300 min, after which the adsorbent material was separated from the filtrate and the concentrations of Congo red dye were measured, then the precipitate was washed by adding (25 ml) of a saline solution (3%) sodium chloride to remove the remaining ethanol on the adsorbent surfaces [30].

Equation (6) was used to calculate the recovery ratio ($S\%$) [31]:

$$S\% = \frac{C_d V_d}{Q_e m} \times 100, \tag{6}$$

where:

$S\%$ = percentage recovery of adsorbent.

V_d = volume of solution in (l).

C_d = concentration of solution after reactivation, in (mg l^{-1}).

Q_e = gravimetric capacity of adsorption in (mg g^{-1}).

m = weight of the absorbing surface (g).

3. Results and discussion

Figure 1(a) shows several peaks of the spectrum of the prepared compound Within the values (400–4000 cm^{-1}). The spectrum showed a peak at 573.99 cm^{-1} Returning to the amplitude vibration of (Fe–O) bond [32]. A group of peaks appeared within the range 600–400 cm^{-1} Returning to the amplitude vibration of (Co–O) and (Cr–O) bonds [33]. A peak appeared at 919.90 cm^{-1} due to the nitrate group [34].

Figure 1(b) showed the XRD spectrum of the single crystal phase of the prepared sample, the spectrum also showed the spin phase of the prepared ferrite as well as the presence of a group of peaks in with angular range (θ = 0–80) in locations: (30.37, 35.90, 37.50, 43.49, 53.98, 57.39, 63.14, 71.65 and 74.64). The results were compared with the international card (JCPDS file No. 22-1086) to prove the formation of ferrite $Co_{0.5}Cr_{0.5}Fe_2O_4$, and the results agreed with the work of the researcher Beera and his group [35]. Through the Debye–Scherrer equation (equation (7)), the crystal sizes of the compound were calculated through the value of (FWHM) which represents the width of the band at the middle of the highest peak.

$$\tau_{hkl} = (K \times \lambda)/(\beta_{hkl} \times \cos\theta_{hkl}), \tag{7}$$

where: τ represents the size of the normal line of the plane (hkl) of the parallel particle, K value (0.9) where represents the wavelength of x-rays, λ is the wavelength of (K-alpha and equals) (1.5406 Å) for copper, β_{hkl} represents the full width at half maximum, θ is the angle of incidence of x-rays in units of the radial angle [36]. The results showed that the value of the crystal size of the nanocomposite is about (28.34 nm) for the prepared compound.

The images showed the compound to be semi-spherical in shape. The images also showed that there is agglomeration in the prepared compounds and that the surface of the compounds contains many pores or holes. Since these pores will increase the surface area of the compound, it is expected that these holes will play an important role in enhancing the adsorption process of heavy elements on the

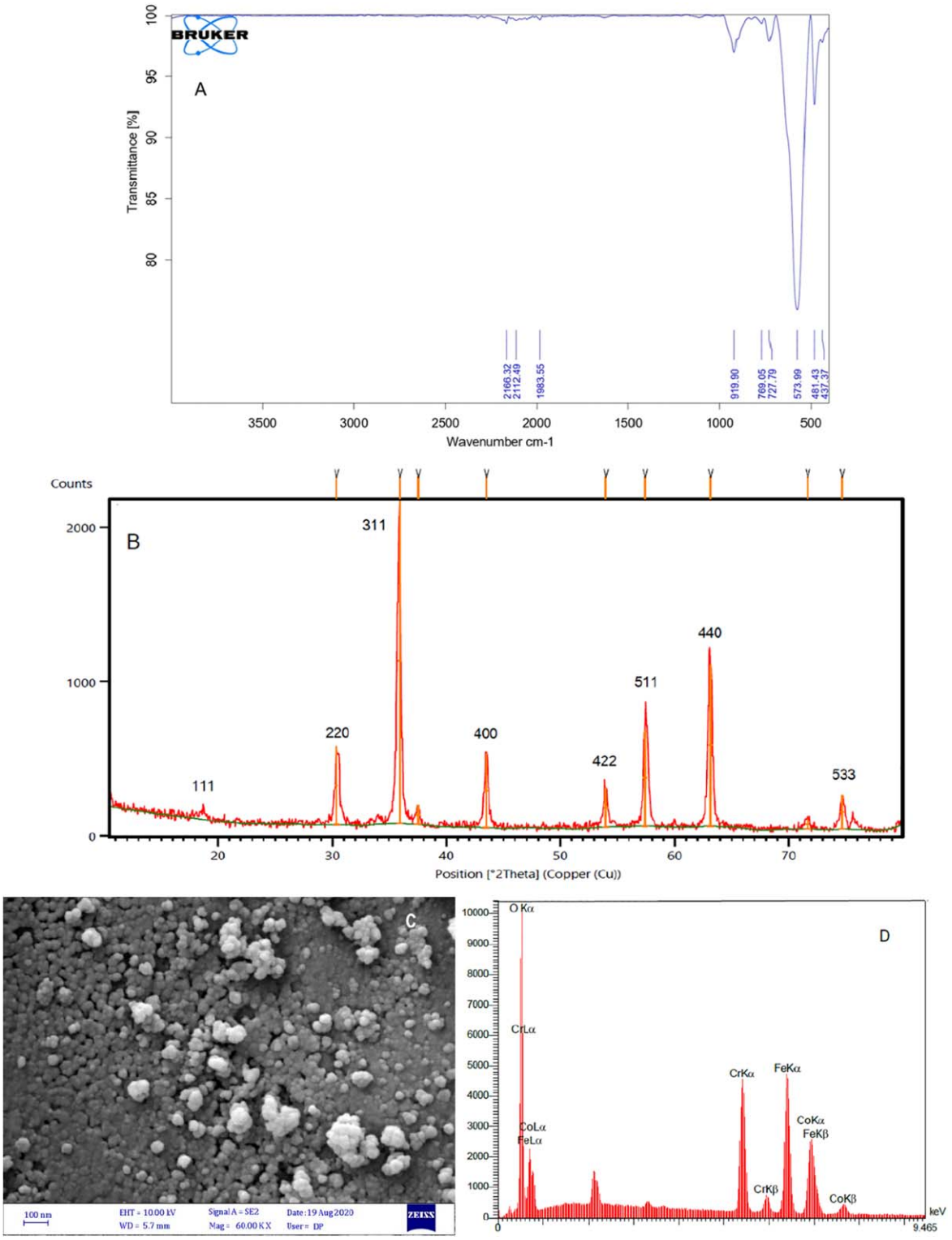

Figure 1. (a) FT-IR spectra, (b) XRD spectrum ,(c) FESEM images and (d) EDX spectra of $Co_{0.5}Cr_{0.5}Fe_2O_4$.

surface of the adsorbent. It is also clear from the figures that the prepared compounds have crystal sizes within the nano range. The (Image-J) program was used to determine the granules and calculate their sizes through image analysis. After determining the shape of the granules through the summary obtained from the program, the average granule size was calculated, and its value was (33.57). Through (EDX) analysis, the purity of the compound was confirmed and the EDX spectrum showed that the results were consistent with the theoretical calculations of the ratios of the elements Cr, O and Fe, as shown in figure 1(d), where the practical weight percentage values of iron, chromium, cobalt and oxygen were 43.78, 11.90, 13.98 and 30.34, respectively.

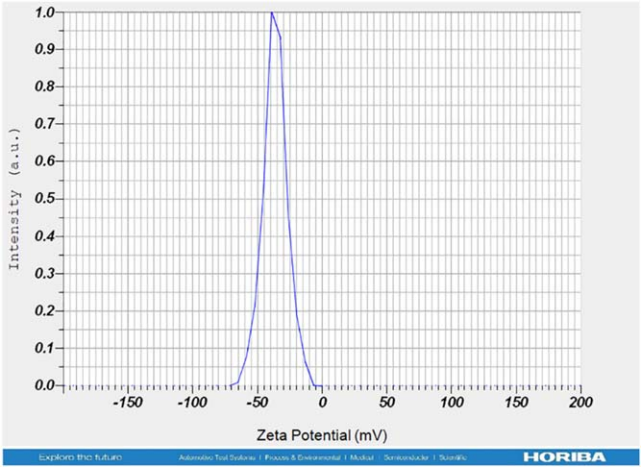

Figure 2. Zeta Potential of $Co_{0.5}Cr_{0.5}Fe_2O_4$.

3.1. Zeta potential study

The stability of the prepared compound was identified and the zeta potential was studied, where the results showed high values. As shown in the figure 2 for the zeta potential of the compound $Co_{0.5}Cr_{0.5}Fe_2O_4$, which reached (−36.3 mV), and this indicates the stability of the compound according to the adiabatic, as the compound is stable if the zeta potential value is positive or negative and higher than ±30 mV, but if the values are less than ±30 mV, it indicates the physical instability of the colloidal compound [37].

3.2. Brunauer–Emmett–Teller (BET)

Determining the surface area of the prepared compounds (adsorbent surfaces) facilitates the process of interpreting the behavior of the adsorbent materials. Evaluating the surface area is one of the most important indicators on the basis of which the adsorbent material and its adsorption efficiency are evaluated.

The surface area, size and diameter of the pores of the prepared compound were determined by the (BET) device (Brunauer, Emmett and Telle) in which nitrogen gas is used for adsorption.

The diameters of the pores of the compound were calculated, where its value was (1.2 nm), the size of the pores was (0.213 $cm^3\,g^{-1}$) and the surface area was (13.784 $m^2\,g^{-1}$). The higher surface area of the $Co_{0.5}Cr_{0.5}Fe_2O_4$ nanoparticles can be attributed to the lower size of the particles. It is noted that the pores in the prepared compound are of the micropores type according to the classification of the International Union of Theoretical and Applied Chemistry [38].

4. Adsorption studies

4.1. Effect of contact time

Investigating the impact of time on Congo red dye removal involved using various time periods (15–360 min) using a temperature of 25 °C.

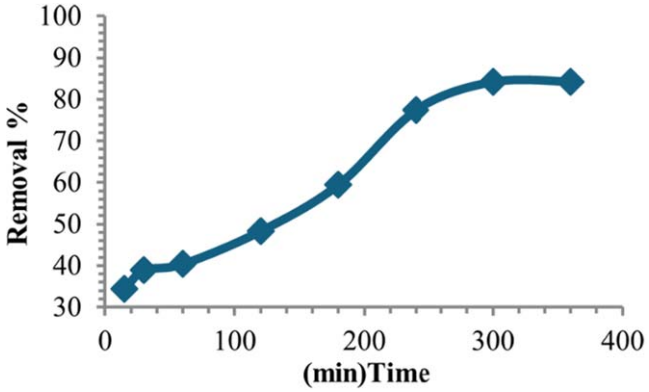

Figure 3. Relationship of the removal percentage to the equilibrium time.

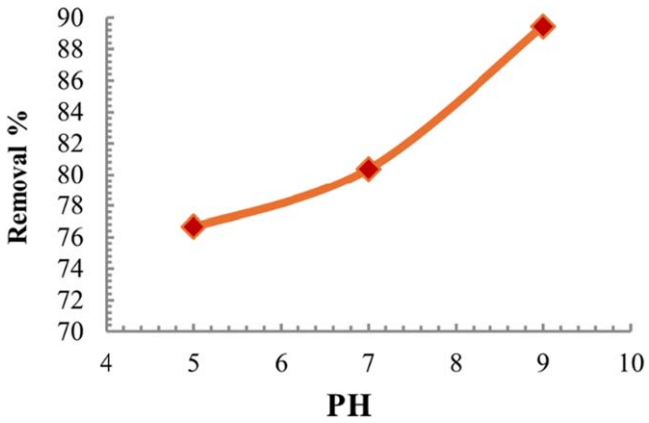

Figure 4. Effect of pH of $Co_{0.5}Cr_{0.5}Fe_2O_4$.

Figure 3 shows that contact time has a significant effect on the dye removal rate, The results of the study showed that the rates of removal of Congo red dye rates increased with increasing contact time until reaching equilibrium [39]. Initially, the amount of absorption was high because it had a large surface area to bind Congo red dye. Towards the end, the adsorption rate slows down, and equilibrium is stabilized due to saturation of the active sites [40, 41]. The equilibrium time has been reached 300 min for $Co_{0.5}Cr_{0.5}Fe_2O_4$. The percentage of the dye removal was found to be 84.24%.

4.2. Effect of pH on the adsorption

The adsorption of Congo red dye at solid-water interfaces is influenced by acidity. pH affects the binding sites of the sorbent and the availability of Congo red in solution [42]. The adsorption of the Congo red dye on $Co_{0.5}Cr_{0.5}Fe_2O_4$ nanoparticle was studied to understand how pH levels (5, 7, and 9) affect it. The study used a fixed concentration of 20 mg l^{-1} at (25 °C) and a time of (300 min). Figure 4 illustrates the effect of pH on the adsorption process.

The results show a clear increase in the percentage of dye removal with increasing acidity, that is, when moving from acidic to basic media, and that the highest percentage of removal of dye was (89.45%) at (pH = 9). The lowest

Table 1. Value of Langmuir and Freundlich constants for the studied system.

Temp. (C)	Langmuir constants			Freundlich constants		
	Q_m (mg g^{-1})	b (l mg^{-1})	R^2	n	K_f	R^2
10.0	12.015	0.545	0.9979	3.811	5.064	0.9698
25.0	12.468	0.701	0.9988	3.935	5.568	0.9510
37.5	13.348	0.784	0.9963	4.197	6.333	0.9718
50.0	14.235	0.914	0.9948	4.580	7.199	0.9891

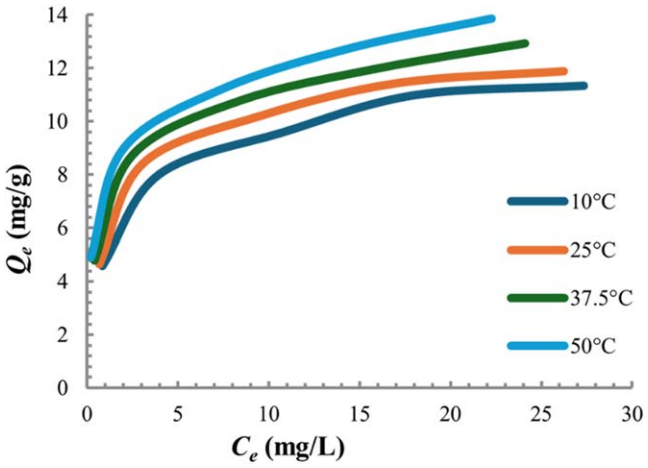

Figure 5. Adsorption isotherm on $Co_{0.5}Cr_{0.5}Fe_2O_4$ nanoparticles at various temperatures.

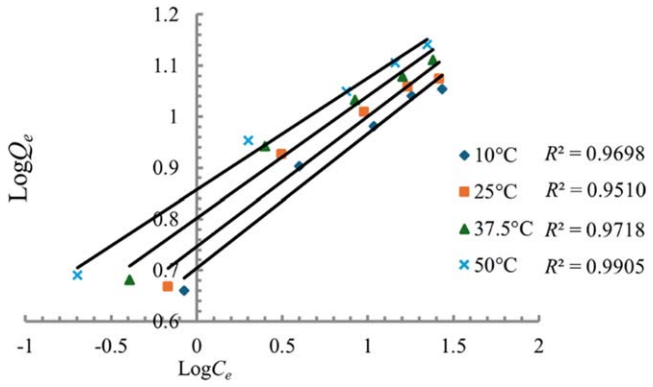

Figure 6. The Freundlich isotherms linear form of the dye on $Co_{0.5}Cr_{0.5}Fe_2O_4$ nanoparticles at various temperatures.

percentage of removal was (76.65%) at (pH = 5) because the basic dye (Congo red) gives off positively charged ions when dissolved in water. At low pH levels, hydrogen ions (H^+) will increase, and thus the hydrogen ions will compete with the positive charge of the cationic (positively charged) dye for the negatively charged sites on the surface of the absorbent, which will lead to a decrease in the percentage of removal. However, at lofty acid levels, the surface of the absorbent will gain a negative charge, and then there will be an increase in the percentage. The absorption rate is due to the increased electrostatic attraction between the negatively charged surface of the sorbent and the positively charged dye molecules [43].

4.3. Adsorption isotherm

Four temperatures were selected in the range (10, 25, 37.5, 50 °C) to determine the ability of the prepared compound $Co_{0.5}Cr_{0.5}Fe_2O_4$ to remove the dye. Figure 5 shows the isothermal absorption of Congo red dye.

The lead ion adsorption isotherm form on the $Co_{0.5}Cr_{0.5}Fe_2O_4$ nanostructures conforms to the (L-type) of Gills classification. L-curve, it indicates that the direction of the molecules adsorbed on the adsorbent surface is horizontal, meaning that the major axis of the adsorbent is parallel to the surface of the adsorbent, such as the adsorption of carbon chains or cyclic hydrocarbons [44]. The Freundlich and the Langmuir equation were used to analyze the experimental adsorption results. Equations (8) and (9) represent the Freundlich and Langmuir equations, respectively [45]. Table 1 shows the isothermal data of the adsorbents.

$$\log Q_e = \log K_f + 1/n \log C_e \tag{8}$$

n, K_f Freundlich constants where represent adsorption capacity and adsorption density respectively.

$$C_e/Q_e = 1/Q_m b + C_e/Q_m, \tag{9}$$

where Q_m is the utmost adsorption capacity (mg g^{-1}) and b is Langmuir constant

The experimental information for the adsorption of dye onto $Co_{0.5}Cr_{0.5}Fe_2O_4$ nanoparticles are analyzed using Langmuir and Freundlich equations, with C_e/Q_e versus C_e plotted and log Q_e versus logC_e, respectively figures 6, 7. The R^2 values closer to one for the Freundlich model than the Langmuir model are shown in table 1, This demonstrates that the Langmuir model is more applicable to describing the adsorption of Congo red dye onto $Co_{0.5}Cr_{0.5}Fe_2O_4$ than the Freundlich models, making it the more accurate method for describing monolayer adsorption on a uniform adsorption surface [46].

4.4. The study of thermodynamics

The effect of temperature on the adsorption of dye at different concentrations and over a range of temperatures from (10 °C–50 °C) was analyzed and the following functions (ΔG), (ΔH) and (ΔS) were calculated and shown in table 2.

Through the results, it was found that there is a linear relationship between $1/T$ and ln$K$ and the correlation

Table 2. Results of using thermodynamic function for absorption both of the Congo red dye.

	K				$-\Delta G$					
	Temperature									
Co (mg l^{-1})	283	283	310.5	323	283	298	310.5	323	ΔH	ΔS
10	10.904	10.904	23.752	48.019	−5.119	−6.874	−8.336	−9.799	27.992	0.117
20	4.025	4.025	6.974	8.910	−3.040	−4.000	−4.800	−5.600	15.072	0.064
30	1.772	1.772	2.561	2.987	−1.055	−1.640	−2.127	−2.615	9.982	0.039
40	1.217	1.217	1.498	1.759	−0.207	−0.567	−0.867	−1.167	6.585	0.024
50	0.829	0.829	1.073	1.245	0.737	0.362	0.050	−0.263	7.812	0.025

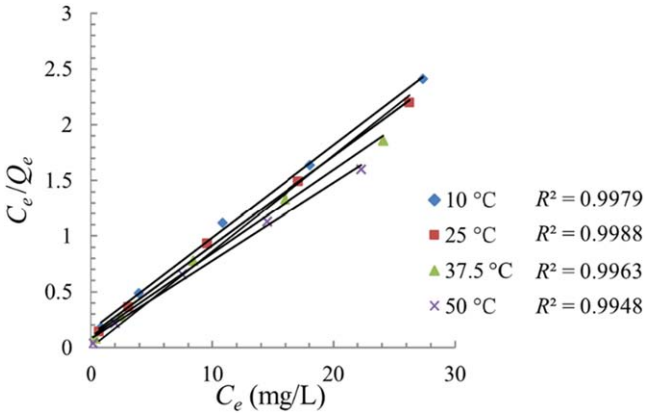

Figure 7. The Langmuir isotherms linear form of the dye on $Co_{0.5}Cr_{0.5}Fe_2O_4$ nanoparticles at various temperatures.

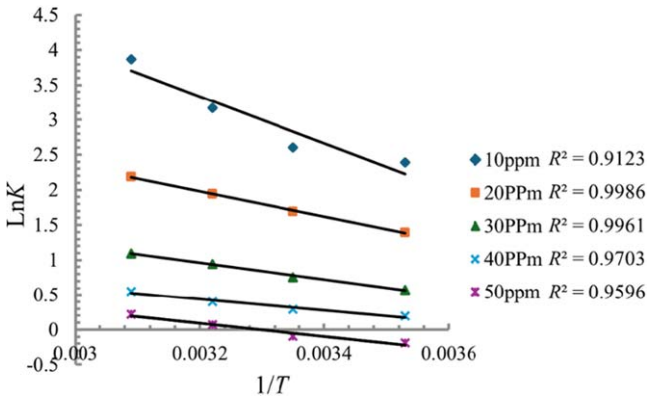

Figure 8. Plot of ln$K$ against $1/T$ for adsorption of the Congo red dye on $Co_{0.5}Cr_{0.5}Fe_2O_4$.

Table 3. Comparison of the prepared nanosurface with other adsorbent nanosurfaces.

Nano—adsorbent	Q_m (mg g^{-1})	References
magnetic nano-alumina	27.397	50
Copper Oxide	0.35	51
zinc oxide	9.615	52
$CoFe_2O_4$	13.88	53
$Co_{0.5}Cr_{0.5}Fe_2O_4$	14.235	The present study

coefficient ($R^2 = 0.9123$–0.9986) for the Congo red dye adsorption on both of $Co_{0.5}Cr_{0.5}Fe_2O_4$ nanoparticles (figure 8).

Figure 8 shows the plot of $1/T$ versus ln$K$ for the adsorption of Congo red dye onto $Co_{0.5}Cr_{0.5}Fe_2O_4$ nanoparticles. According to table 2, the enthalpy (ΔH) results for the adsorption of dye onto $Co_{0.5}Cr_{0.5}Fe_2O_4$ nanoparticles showed positive values indicating an endothermic adsorption process, and a positive results of ΔS was observed during the adsorption process, and the interaction between solid and liquid became more random [47, 48]. As for the value of ΔG, with increasing the concentration of the absorbent material, the thermodynamic function ΔG changed from negative to positive after showing negative values at lower concentrations [49].

The adsorption capacity of the prepared nanomaterial was compared with some nanosurfaces for adsorption of Congo red dye, as shown in table 3.

4.5. Activate adsorbent surfaces

The reactivation process of the adsorbent surfaces is of utmost importance for the purpose of using them multiple times, so the reactivation process was studied where the reactivation rate was very high as the recovery rate in the first activation process for all experimental samples reached (98.65%), and (96.93%) in the second activation process where it decreased slightly, and the results indicate the possibility of reusing the adsorbent surface multiple times with the possibility of maintaining its high ability to adsorb the studied pollutants, and the reason for separating the Congo red dye in ethyl alcohol is that it works to remove the adhesion of the absorbent materials to the surfaces of the absorbent material [50].

The present study showed a decrease in adsorption efficiency upon the second activation. The decrease in adsorption efficiency can be attributed to surface contamination during the adsorption process. Contaminants can accumulate on the surface of the adsorbent and the accumulation leads to blocking of the active sites, which are essential for the adsorption process. Also, the accumulation of contaminants can create a layer that hinders the access of the adsorbent to the active sites, thus reducing the surface's ability to adsorb the adsorbents. Secondary contamination can also occur

during the activation process, as the remaining contaminants from previous cycles may not be completely removed, leading to a gradual decrease in adsorption efficiency over time [51].

5. Conclusion

This research involved the use of sol–gel self-combustion method to prepare $Co_{0.5}Cr_{0.5}Fe_2O_4$ nanoparticles, using lemon juice extract as surfactant and fuel agent. To produce single-phase ferrite, the sample was heated to 600 °C. The spectra of the prepared samples showed single-phase and crystalline characteristics. The absorption isotherms were calculated and were accurately represented by both Langmuir and Freundlich models, with the Langmuir model having a better fit than the Freundlich model. According to the thermodynamic properties, the adsorption reaction was spontaneous and endothermic. Therefore, the compound can be used as an adsorbent for Congo red dye in environmental applications for environmental protection, as the results showed a spontaneous reaction as well as an endothermic reaction through thermodynamic results. In future works, other organic and inorganic pollutants such as (heavy elements and petroleum hydrocarbons) will be selected and removed from polluted water (industrial and marine water).

References

[1] Aziz H K H, Mustafa F S, Omer K M, Hama S, Hamarawf R F and Rahman K O 2023 *RSC Adv.* **13** 17595–610
[2] Ajibola V O, Funtua I I and Unuaworho A E 2005 *J. Environ. Sci.* **3** 49–54
[3] Masoud M S, Haggag S S, Heiba H F, Abd El-Hamed O H, Habila N S, Abdel-Hamid I A M and Mohamed L A 2023 *Environ. Process.* **10** 1–27
[4] Sen T K, Afroze S and Ang H 2011 *Water Air Soil Pollut.* **218** 499–515
[5] Yagub M T, Sen T K and Ang H 2012 *Water Air Soil Pollut.* **223** 5267–82
[6] Chan A, Rubiyatno and Akhmetov Z 2024 *Tropical Aquatic Soil Pollut.* **4** 87–99
[7] Liu J, Cheng X Z, Qin P and Pan M Y 2012 *Adv. Mater. Res.* **599** 391–4
[8] Kim H, Park C, Choi N and Cho K 2024 *Environ. Sci. Pollut. Res.* **31** 28443–53
[9] Bhattacharyya K G and Sharma A 2004 *J. Environ. Manage.* **71** 217–29
[10] Mittal A, Mittal J, Malviya A and Gupta V K 2009 *J. Colloid Interface Sci.* **340** 16–26
[11] Khudhair S H and Al-Fayaad D B M 2022 *Iraqi J. Sci.* **36** 4674–82
[12] Sayğılı G A 2015 *J. Mol. Liq.* **211** 515–26
[13] Daoud M, Benturki O, Girods P, Donnot A and Fontana S 2019 *Microchem. J.* **148** 493–502
[14] Taha A A, Kandil S, Mohamed L A, Sallam M G and Heiba H F 2023 *J. Mol. Struct.* **1288** 135716
[15] Singh K K, Singh A and Rai S 2021 *Mater. Today: Proc.* **51** 1157–63
[16] Salman G K, Bohan A J and Jaed G M 2017 *J. Eng. Technol.* **35** 903–8
[17] Kefeni K K, Mamba B B and Msagati T A M 2017 *Sep. Purif. Technol.* **188** 399–422
[18] Chinh V T, Dang V Q, Hoai P N, Tuan N T and Duong D 2020 *J. Am. Chem. Soc.* **5** 7298–306
[19] Baig R B N and Varma R S 2013 *Chem. Commun.* **49** 752–70
[20] Nasir Baig R B, Nadagouda M N and Varma R S 2015 *Coord. Chem. Rev.* **287** 137–56
[21] Roonasi P and Nezhad A Y 2016 *Chem. Phys.* **172** 143–9
[22] Dutta S K, Akhter M, Ahmed J, Amin M K and Dhar P K 2022 *Biointerface Res. Appl. Chem.* **12** 4399–416
[23] Mahboubeh H, Fatemeh Z, Zahra J R and Zohreh A 2014 *J. Magn. Magn. Mater.* 37143–8
[24] Hammood A Y, Mohammed I K and Majeed A A 2023 *Pollution* **9** 994–1005
[25] Zhao D, Wu X, Guan H and Han E 2007 *J. Supercrit Fluids* **4** 226–33
[26] Sivakumar M, Kanagesan S, Babu R S, Jesurani S and Velmurugan R 2012 *J. Mater. Sci.: Mater. Electron.* 231045–9
[27] Jaafar R S and Hammood A Y 2024 *Pollution* **10** 63–72
[28] Jain P, Kaur M, Kaur M and Grewa J K 2019 *Bull. Mater. Sci.* **77** 1–9
[29] Ge H and Ma Z 2015 *J. Carbo. Poly* **131** 280–7
[30] Perez E, Marquez G and Sagredo V 2019 *Iraqi J. Appl. Phys.* **15** 13–7
[31] Theurer J 2019 *MSc thesis* Oklahoma University—USA
[32] Soldatkina L and Zavrichko M 2019 *Colloids Interfaces.* **3** 4–16
[33] Shaima'a J K and Ali A H 2018 *J. Univ. Babylon, Engin. Sci.* **26** 282–91
[34] Ghasemi A 2015 *J. Alloys Compd.* **645** 467–77
[35] Beera C S *et al* 2023 *Gels J.* **9** 110873
[36] Cullity B D 1978 *Elements of X-Ray Diffraction* (Addison-Wesley) 2nd edn
[37] Mohammed I, Al-Shehri D, Mahmoud M, Kamal M S and Alade O S 2021 *ACS Omega* **6** 4022–33
[38] Thommes M, Kaneko K, Neimark A V, Olivier J P, Rodriguez-Reinoso F, Rouquerol J and Sing K S W 2015 *Pure Appl. Chem.* **87** 1051–69
[39] Taha A A, Shreadah M A, Heiba H F and Ahmed A M 2017 *Asia-Pac. J. Chem. Eng.* **12** 292–306
[40] El-Ashtoukhy E, Amina N K and Abdelwahab O 2008 *J. Desalination* **223** 162–73
[41] hlivan E, Altun T and Parlayıcı S 2009 *J. Hazardous Mater.* **164** 982–6
[42] Esposito A, Pagnanelli F and Veglio F 2002 *J. Chemi. Engin. Scie.* **57** 307–13
[43] Porkodi K and Kumar K V 2007 *J. Hazardous Mater.* **143** 311–27
[44] Giles C H, MamEwans T H, Nakhwa S N and Smith D 1960 *J. Chem. Soc.* **786** 3973–93
[45] Hammood A Y, Tememi A L-, Abdulnabi M K and Majed Z A A A 2024 *Adv. Nat. Sci.: Nanosci. Nanotechnol.* **15** 045015
[46] Barrow G M 1994 *Physical Chemistry* 5th edn (McGraw-Hill) pp 310–44
[47] Abdel-Khalek A A, Abdel-Hafeez M M, Mohamed R A and Gabrail E H 2022 *Egypt. J. Chem.* **65** 189–99
[48] Heiba H F, Taha A A, Mostafa A R, Mohamed L A and Fahmy M A 2020 *Int. J. Biol. Macromol.* **152** 554–66
[49] Hefne J A, Mekhemer W K, Alandis N M, Aldayel O A and Alajyan T 2008 *Int. J. Phys. Sci.* **3** 281–8
[50] Cheng C, Liu Z, Li X, Su B, Zhou T and Zhao C 2014 *RSC Adv.* **4** 42346–57
[51] Alsawy T, Rashad E, El-Qelish M and Mohammed R H 2022 *Npj Clean Water* **5** 1–21